Korean J. Chem. Eng., 40(10), 2555-2564 (2023)
DOI: 10.1007/s11814-023-1527-7

pISSN: 0256-1115
eISSN: 1975-7220

Melamine-benzaldehyde tris-schiff base as an efficient corrosion inhibitor for mild steel in 0.5 molar hydrochloric acid solution: Weight loss, electrochemical, theoretical and surface studies

Ifzan Arshad*,,†, Khizar Qureshi***, Shern-Long Lee*,†, Safia Khan****, Muhammad Amin Abid*****, Awais Bokhari******, Aboud Ahmed Awadh Bahajjaj*******, and Muhammad Naeem Ahmed********

*Institute for Advanced Study, Shenzhen University, Shenzhen, Guangdong 518060, P. R. of China
**College of Civil and Transportation Engineering, Shenzhen University, Shenzhen, China
***Department of Chemistry, University of Management and Technology, Sialkot, Pakistan
****Shandong Technology Centre of Nanodevices and Integration, School of Microelectronics, Shandong University, Jinan 25101, China
*****Department of Chemistry, University of Sahiwal, Sahiwal Pakistan
******Sustainable Process Integration Laboratory, Faculty of Mechanical Engineering, Brno University of Technology, 2896/2,61600, Brno, Czech Republic
*******Department of Chemistry, College of Science, King Saud University, Riyadh 11451, Saudi Arabia
********Department of Chemistry, The University of Azad Jammu and Kashmir, Muzaffarabad 13100, Pakistan
(*Received 29 January 2023 • Revised 5 June 2023 • Accepted 5 July 2023*)

Abstract−In the current study, the *N,N′,N″*-(1,3,5-triazine-2,4,6-triyl)tris(1-phenylmethanimine) (MBSB) condensation product of melamine (triazine) and benzaldehyde was investigated as a mild steel corrosion inhibitor in a 0.5 M HCl. The ability of the synthesized tris-Schiff base to suppress corrosion was evaluated utilizing weight loss measurements and electrochemical techniques. The maximum inhibition efficiency of 94.78%, 93.99% and 93.80% was achieved using 100 ppm of MBSB in weight loss measurements, polarization, and EIS tests, respectively. It was observed that increasing inhibitor concentration enhanced inhibition performance, whereas increasing temperature lowered inhibition performance. The analyses demonstrated that the synthesized tris-Schiff base inhibitor followed the Langmuir adsorption isotherm, and the inhibitor was an effective mixed-type inhibitor having a low cathodic predominance. According to the electrochemical impedance measurements, the R_{ct} values increased with the increase of inhibitor concentration. In addition, theoretical calculations using density functional theory (DFT) were performed to reveal the anticorrosion mechanism. The weight loss and electrochemical assessments were also supported by surface characterization analysis and show a substantial smoothness in the surface morphology.

Keywords: Organic Corrosion Inhibitors, Corrosion Inhibition, EIS, Acidic Corrosion, Polarization

INTRODUCTION

Mild steel has a very low cost with excellent mechanical strength, which makes it a popular choice in the petroleum and natural gas industries. Strong acids, such as hydrochloric acid, are utilized for acid descaling, acid pickling, and oil well acidification to eliminate undesired salt deposits and scales that improve oil recovery [1]. However, strong acids may corrode the mild steel's surface, ultimately resulting in expensive repairs and system maintenance and financial, physical, and environmental losses [1-4].

The most popular kind of corrosion inhibitor is organic corrosion inhibitors, which are categorized based on their chemical structure, mechanism of action, and other properties. Their affordability, ease of application, and a high degree of protection have all contributed to their increasing popularity. They adsorb on the surface of metals and protect them from corrosion [5-8], and their effectiveness in a range of acidic solutions is also due to the heteroatoms they contain, such as nitrogen, oxygen, phosphorus, sulfur and halogens [9,10]. Adsorption of the organic molecules onto the surface of metal prevents direct contact between the metals and the corrosive environment [11,12]. Though many organic corrosion inhibitors are costly and harmful for the public health and environment. In an acidic environment, organic molecules containing heterocyclic and aromatic heterocyclic rings exhibit greater corrosion inhibition [13-18]. Organic molecule adsorption is influenced by both chemical and physical bonding. The inhibitors' effectiveness may be attributed to its low electronegativity and great polarizability, which allow covering huge metal surfaces and quickly transferring electrons to vacant atomic orbitals [19]. The triazine ring-containing compound known as melamine has three nitrogen atoms and therefore is a nitrogen-rich molecule [20,21]. These nitrogen atoms are readily protonated, thus increasing the solubility of polar solvents. Melamine derivatives have recently made substantial progress for a range of objectives, including the prevention of

†To whom correspondence should be addressed.
E-mail: arshadmi@mail.ustc.edu.cn, Sllee@szu.edu.cn

corrosion. The remarkable inhibition efficiency of melamine derivatives is attributed to the adsorption of protonated sites and the sharing of electrons and lone pair electrons with the iron atom [20,21]. Also, the presence of a nitrogen and oxygen atom makes isatin derivatives among the hetero-atom-containing compounds quite efficient corrosion inhibitors, and several of isatin derivatives have been discussed in depth as promising corrosion inhibitors for metals [22-24]. Recent research shows a tremendous rise in using Schiff base derivatives as a corrosion inhibitor for metals, including steel, aluminum, and copper in very acidic environments [25-29]. Schiff bases can be easily made from extremely cheap starting materials and have little toxicity; therefore, they are becoming more and more popular as corrosion inhibitors.

The aforementioned factors encouraged us to synthesize melamine-isatin Schiff base and to evaluate the thermodynamic factors affecting the adsorption of compound, namely *N,N′,N″*-(1,3,5-triazine-2,4,6-triyl)tris(1-phenylmethanimine) (MBSB) on the surface of mild steel in acidic environment using weight loss measurements, electrochemical techniques, surface morphology and computational studies.

EXPERIMENTAL

1. Materials and Sample Preparation

Chemicals and solvents of analytical grade were used to synthesize the tris-Schiff base of melamine with benzaldehyde. All the solvents, including melamine and benzaldehyde, were purchased from Sigma Aldrich and used without further purification. 0.5 M HCl solution was prepared in deionized water using analytical-grade hydrochloric acid (37%). Mild steel specimens used in this work mainly contain elemental composition C (0.17%), Mn (1.6%), P (0.040%), Si (0.59%), and Fe (remaining portion). For the weight loss measurements, the specimen of dimensions 2 cm×2 cm×0.3 cm was used. Prior to the studies steel specimen was burnished with emery paper of 600-1,200 grade under a running tap. They were cleaned with deionized water, then degassed with acetone and alcohol followed by drying with cold air. Before tests, the polished mild steel specimens were kept in a vacuum desiccator.

2. Synthesis and Characterization Data of MBSB

The Schiff base *N,N′,N″*-(1,3,5-triazine-2,4,6-triyl)tris(1-phenylmethanimine) (MBSB), as shown in Scheme 1, was synthesized by the condensation reaction between melamine (10 mmol, 1.26 g) with 3-fold of benzaldehyde (30 mmol, 3.18 g, 3.05 ml) in ethanol as solvent under reflux for about 4 hr at temperature (100-120 °C) during which a solid compound was separated. It was filtered and washed with cold ethanol followed by drying in vacuum oven yielding 89% MBSB as pure product.

N,N′,N″-(1,3,5-triazine-2,4,6-triyl)tris(1-phenylmethanimine) (MBSB) Yield: 89%, elemental analysis: calc.: C, 71.78; H, 4.30; N, 23.92; found: C, 71.72; H, 4.27; N, 23.85%; characteristics IR peaks (ATR): υ N-H=3,513, υ C-H (aromatic)=3,062, υ C=O=1,705, υ C=N=1,640 cm^{-1}; 1H NMR (400 MHz, DMSO, δ, ppm) δ=8.95 (s, 3H, NH), 7.77-7.43 (m, 6H, Ar-H), 7.58-7.50 (m, 9H, Ar-H); ^{13}C NMR (100 MHz, DMSO, δ, ppm) δ=170.36 (C=O), 168.68 (C=N, triazine), 136.68, 132.57, 129.64, 128.61.

3. Weight Loss Measurements

Because of its outstanding accuracy, easiness, and excellent repeatability, the weight loss method was used to examine the corrosion protection behavior initially. The weighted metallic specimens with dimensions of 2.0×2.0×0.3 cm were allowed to corrode in the 50 mL of 0.5 M HCl without and with the varying concentrations of MBSB for the immersion time of 4 hours in a thermostatically controlled water bath TW-2.02 (Thomas Scientific). These specimens were taken out after a particular duration of time, and the corrosion products on them were gently wiped off with water and acetone. To ensure the measurement's reproducibility, a weight loss experiment was carried out in triplicate using KERN ABS-N analytical balance with readability up to 0.01 mg for each investigated concentration of MBSB. The following equations were used to determine the rate of corrosion and inhibition efficiency (IE%) [1,30].

$$C_R(mgcm^{-2}h^{-1}) = \frac{\Delta w}{st} \quad (1)$$

$$IE\% = \frac{(C_R)_a - (C_R)_p}{(C_R)_a} \times 100 \quad (2)$$

$$\theta = \frac{IE\%}{100} \quad (3)$$

where, IE%, C_R ($mgcm^{-2}h^{-1}$), and θ denote the inhibition efficiency (%), rate of corrosion, and the surface coverage, respectively. The rates of corrosion for uninhibited and inhibited conditions, respectively, are $(C_R)_a$ and $(C_R)_p$. s is the surface area in cm^2, and t is the exposure duration (4 h). Δw stands for the difference between the initial and final weight of the specimens at different concentrations under study.

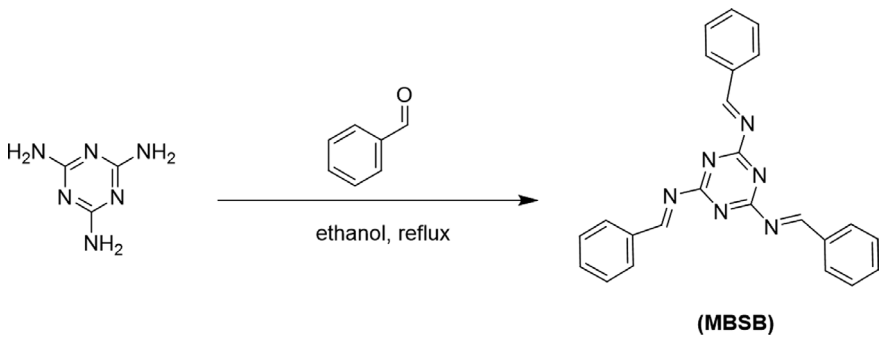

Scheme 1. Synthetic Scheme for MBSB inhibitor molecule.

4. Electrochemical Measurements

The electrochemical workstation CHI660D was employed for electrochemical (EIS and PDP) studies. The nature of electrodes and method used to prepare them were similar to those reported in our previous paper [1]. After half an hour of immersion, the electrochemical experiments were run. The establishment of open circuit potential (OCP) necessitated almost a 30 min immersion. EIS data were recorded by employing 10 mV signal between 0.01 Hz to 100 kHz frequency. By fitting the Nyquist curves of metallic specimens that were both inhibited and uninhibited, values for polarization resistance (R_p) were obtained and then percentage inhibition (IE%) was then calculated by using the following formula [1,6].

$$IE\% = \left(1 - \frac{R_P^a}{R_P^p}\right) \times 100 \quad (4)$$

In Eq. (4), R_P^a and R_P^p are the polarization resistances in the absence and in the presence of synthesized inhibitor. Working electrode potentials against the corrosion potential (E_{corr}) for the potentiodynamic polarization study were permitted to vary from 250 mV to +250 mV. To get the values of corrosion current density (i_{corr}), the linear Tafel curve sections were extrapolated. The percentage inhibition (IE%) by using these values is calculated by Eq. (5) [1,5].

$$IE(\%) = \frac{i_{corr}^o - i_{corr}}{i_{corr}^o} \times 100 \quad (5)$$

where i_{corr} and i_{corr}^o are the corrosion current densities in the absence and in the presence of inhibitors, respectively.

5. Computational Calculations

The density functional theory (DFT) method was employed to calculate the quantum parameters of our investigated inhibitor MBSB. The geometrical structure of the prepared inhibitor was optimized using Becks three-parameter exchange functional B3 with Lee-Yang-Parr (LYP) non-local correlation functional with 6-321 + G basis set. The molecules were created using Gauss View, 6.0 executed in Gaussian 09 program package [31,32]. Key parameters like the energy of the highest occupied molecular orbital (E_{HOMO}) and the energy of the lowest unoccupied molecular orbital (E_{LUMO}), energy gap (ΔE) between E_{LUMO} and E_{HOMO}, electronegativity (χ), hardness (η), softness (σ) fraction of transferred electrons (ΔN) were also calculated by the following formulas [33-35].

$$\text{Ionization Potential (I)} = -E_{HOMO} \quad (6)$$

$$\text{Electron affinity (A)} = -E_{LUMO} \quad (7)$$

$$\text{Electronegativity } (\chi) = (I+A)/2 \quad (8)$$

Table 1. Weight loss measurements parameters without and with varying concentrations of MBSB inhibitor molecules

Inhibitor	C (ppm)	C_R (mgcm^{-2}h^{-1})	IE%	θ
Blank		5.85		
MBSB	25	1.92	67.03	0.66
	50	1.02	82.37	0.81
	75	0.59	89.70	0.88
	100	0.29	94.78	0.94

$$\text{Electronic hardness } (\eta) = (I - A)/2 \quad (9)$$

$$\text{Chemical softness } (\sigma) = 1/\eta \quad (10)$$

$$\Delta n = \frac{\chi_{Fe} - \chi_{Inhibitor}}{(\eta_{Fe} + \eta_{Inhibitor})} \quad (11)$$

6. Surface Studies

To analyze the surface, cleaned and dried specimens were immersed in 100 mL of 0.5 M HCl for 4 hours, both with and without the addition of MBSB at the optimum concentration. Samples were then cleaned, dried, and subjected to SEM analyses for surface morphological studies. FEI Quanta 450 Field emission scanning electron microscope was used to take the SEM images of inhibited and uninhibited specimens.

RESULTS AND DISCUSSION

1. Weight loss Measurements

1-1. Effect of Concentration

Table 1 shows the variation in IE% values with MBSB molecule concentrations in the acidic dissolution of mild steel. The results show that MBSB's ability to protect from corrosion increases as concentrations increase, attaining its highest efficiency at 42.80×10^{-8} mM concentration. A careful examination of Table 1 indicates that the protective ability significantly improved as concentration of MBSB was increased from 25 to 100 ppm. However, there was only a little rise in the IE% when their concentration was increased from 75 to 100 ppm. These findings indicate that the optimum concentration for MBSB is 75 ppm. The synthesized compound could prevent corrosion because it contains enough free electrons, including a lone pair on nitrogen, electron pair of carbonyls, and these electrons are tightly bound to the positively charged metal surface [1,12,36].

1-2. Effect of Temperature

Table 2 shows how temperature affects the MBSB's capacity to

Table 2. The values of rate of corrosion (C_R), inhibition efficiency (IE%), adsorption constant (K_{ads}), and Gibb's free energy (ΔG_{ads}) for mild steel in 0.5 M HCl at different temperatures

Temperature (k)	Blank	MBSB			
	C_R	ΔG_{ads} (kJ mol^{-1})	$K_{ads}\times10^4$ (L mol^{-1})	C_R	IE %
308	5.87	−35.90	2.19	0.31	94.88
318	8.21	−35.20	1.11	0.82	90.23
328	12.42	−35.18	0.70	1.71	86.01
338	16.64	−34.24	0.33	4.23	74.67

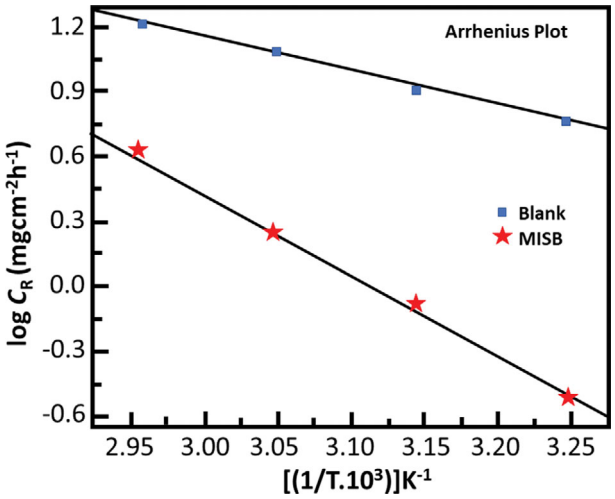

Fig. 1. Arrhenius plots for the corrosion of mild steel in the presence and absence of MBSB.

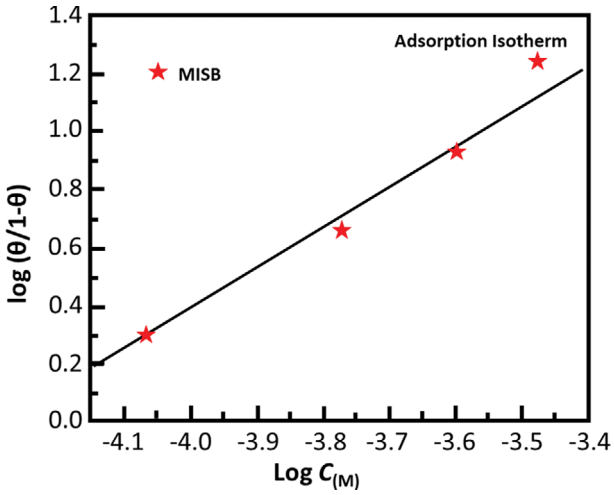

Fig. 2. Langmuir adsorption isotherm plotted for the adsorption of MBSB on mild steel surface in 0.5 M HCl.

prevent the acidic dissolution of mild steel. The findings show that the inhibition efficiency of synthetic inhibitor molecules is deteriorating, and a corresponding rise in corrosion rate values has been seen as temperature has increased. Numerous high temperature-related processes, including molecular fragmentation, acid-catalyzed molecular rearrangement, desorption and molecular etching of adsorbed MBSB inhibitor molecules, are thought to be the cause of MBSB's decreased ability to protect [1,37]. The increase in kinetic energy at higher temperatures causes the desorption of adsorbed inhibitor molecules from the surface of metal, and the force constant between the inhibitor molecules and the metal surface is thus reduced as a result [38]. The most popular method for describing the impact of temperature on the interactions of inhibitor with metal is the Arrhenius equation, which can be written as [1]

$$\mathrm{Log}(C_R) = \frac{-E_a}{2.303RT} + \log A \tag{6}$$

where E_a, A, R, and T, stand for the activation energy, Arrhenius pre-exponential factor, the universal gas constant, and the absolute temperature, respectively. The slopes of Arrhenius plots (Fig. 1) were used to calculate the E_a values. E_a was calculated to be 75.25 kJ mol^{-1}. While the E_a value was just 30.5 kJ mol^{-1} when there were no MBSB molecules present. The adsorption and formation of a defensive barricade by molecules of inhibitor is the cause of the elevated values of activation energy for inhibited conditions. By adhering to the surface, the inhibitor molecules produced a coating that improved the energy barrier for the corrosion process.

2. Adsorption Isotherms

The adsorption isotherm model serves as the most accurate representation of the MBSB interactions with metallic surfaces [1, 12]. To illustrate the adsorption behavior of the synthesized MBSB inhibitor on the surface, some common isotherms were tested in order. Fig. 2 displays the Langmuir adsorption isotherms plot. By using the Langmuir adsorption isotherm equation presented below, the values for the adsorption constants at the optimal concentration of MBSB at various temperatures were evaluated.

$$K_{ads}C = \frac{\theta}{1-\theta} \tag{7}$$

where, C stands for the molar concentration of MBSB molecules, and θ stands for the degree of surface coverage. A high K_{ads} value typically reflects a strong ability for absorption. Table 2 displays the calculated K_{ads} values for the various examined temperatures. The G_{ads} is determined for each temperature by using Eq. (8).

$$\Delta G^{o}_{ads} = -RT\ln(55.5K_{ads}) \tag{8}$$

where the numeral 55.5 stands for the water concentration in acidic solution and further symbols have their conventional meanings. Table 2 also illustrates the calculated K_{ads} values. As can be observed, MBSB has a very high negative value of G_{ads}, which indicates that it has a significant capacity for adsorption [1]; also, the significant tendency of adsorption on the metallic surface was indicated by the high values of K_{ads} for MBSB.

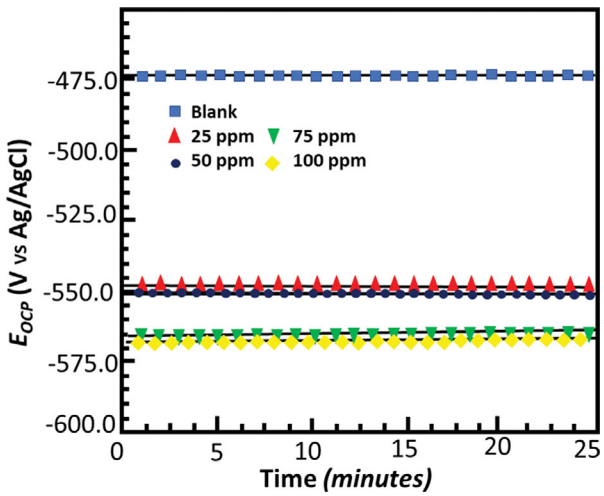

Fig. 3. Open circuit potential vs time curve for corrosion of mild steel in 0.5 M HCl in the absence and presence of various concentrations of MBSB molecules.

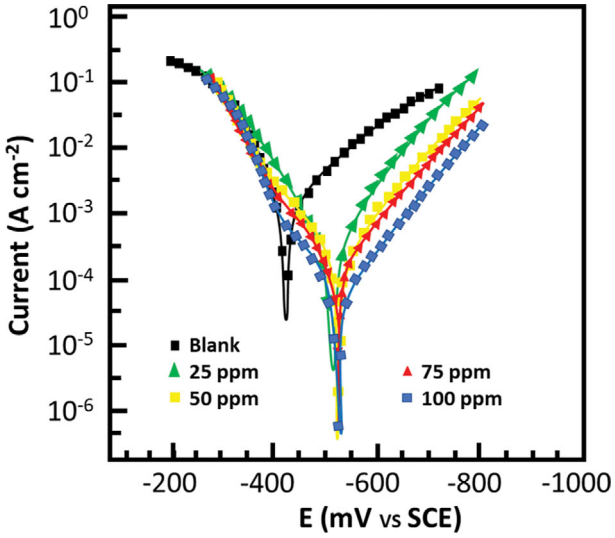

Fig. 4. Polarization curve of mild steel in 0.5 M HCl with and without MBSB molecules.

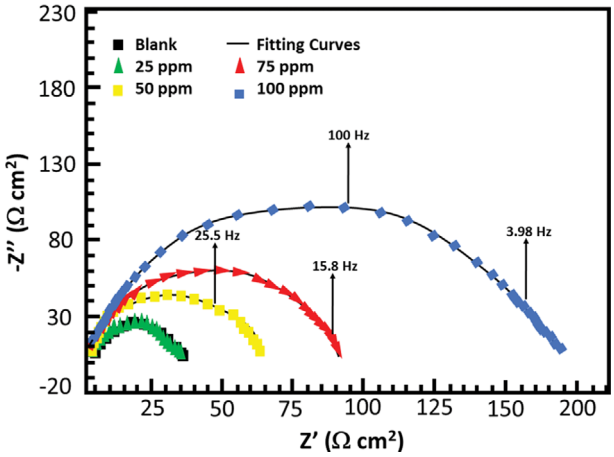

Fig. 5. Nyquist plots for corrosion of mild steel in 0.5 M HCl without and with various concentrations of MBSB molecules.

3. Open Circuit Potential Test

To support the weight loss experiment, electrochemical measurements were conducted. The open circuit potential is the difference between the potentials of the working electrode and the standard or reference electrode when no external current is applied. Fig. 3 displays the open circuit potential versus time curves for 25-minute curves following a half hour immersion. As can be observed, OCP vs time curves for inhibited and uninhibited conditions depict straight lines, indicating that steady state potential has developed in both cases. The straight lines also show that the Fe_2O_3 and Fe_3O_4 oxide layers were entirely eliminated, and that a protective or inhibitive film by the MBSB inhibitor had formed on the surface of metal. Additionally, it can be shown that the open circuit potential vs time curves are shifted with MBSB in a cathodic or negative direction. This result indicates that although the presence of MBSB affects both cathodic and anodic processes, their effectiveness towards cathodic reactions is comparatively higher due to the precipitation of inhibitors molecules on cathodic sites of the surface of metal.

4. Potentiodynamic Polarization Studies

For a thorough insight into inhibitor behavior in their bias toward the anodic and cathodic processes, potentiodynamic polarization studies were conducted. Fig. 4 depicts the cathodic and anodic polarization curve for metallic dissolution in 0.5 M HCl with and without MBSB, and Table 3 lists the polarization indices for inhibitor. It is clear that MBSB, at the various concentrations that were tested, had an impact on both cathodic and anodic reactions and processes, causing a significant drop in values of corrosion current densities (i_{corr}) without altering the typical Tafel curve appearance. This observation revealed that MBSB molecules hinder the process of corrosion by blocking the surface-active sites through adsorption [39]. This data implies that examined inhibitor precipitates over cathodic region and subsequently behave as mostly cathodic type inhibitor since corrosion potential (E_{corr}) for Tafel curve inhibited by MBSB is pushed towards negative site [40]. The shift in value of corrosion potential of the inhibited Tafel curve relative to the uninhibited Tafel curve can be used to characterize the cathodic and/or anodic nature of synthesized inhibitor.

5. Electrochemical Impedance Spectroscopy

Figs. 5 and 6 show the Nyquist and the Bode plots for the corrosion of mild steel in acidic conditions with and without MBSB molecules. At all concentrations under investigation, the Nyquist plots appear as a single semicircle, which suggests a single charge transfer reaction. It is evident that the diameters of the Nyquist plots' semicircles are larger for inhibited metallic specimens than for uninhibited metallic specimens (blank). Additionally, at larger concentrations of MBSB, the diameter of the semicircle increases more noticeably. The Nyquist plots of metallic samples in inhibited and uninhibited conditions were fitted into the suitable equivalent circuit to derive various impedance characteristics. In the described circuit, a constant phase element (CPE) has been used in place of a pure capacitor since it gives a greater understanding on the interactions between metal and electrolyte at interfaces. The following is a presentation of the impedance of the constant phase element,

Table 3. Polarization parameters for the corrosion of mild steel in 0.5 M HCl without and with various concentrations of MBSB molecules

Inhibitor	C (ppm)	E_{corr} (mV/SCE)	β_a (μA/cm^2)	β_c (mV/dec)	i_{corr} (mV/dec)	IE%	θ
Blank		−446	70.5	114.7	1,129		
MBSB	25	−531	127.7	96.9	385	65.83	0.64
	50	−544	83.3	81.7	185	83.50	0.82
	75	−453	135.0	148.7	143	87.23	0.86
	100	−541	140.3	176.6	67	93.99	0.92

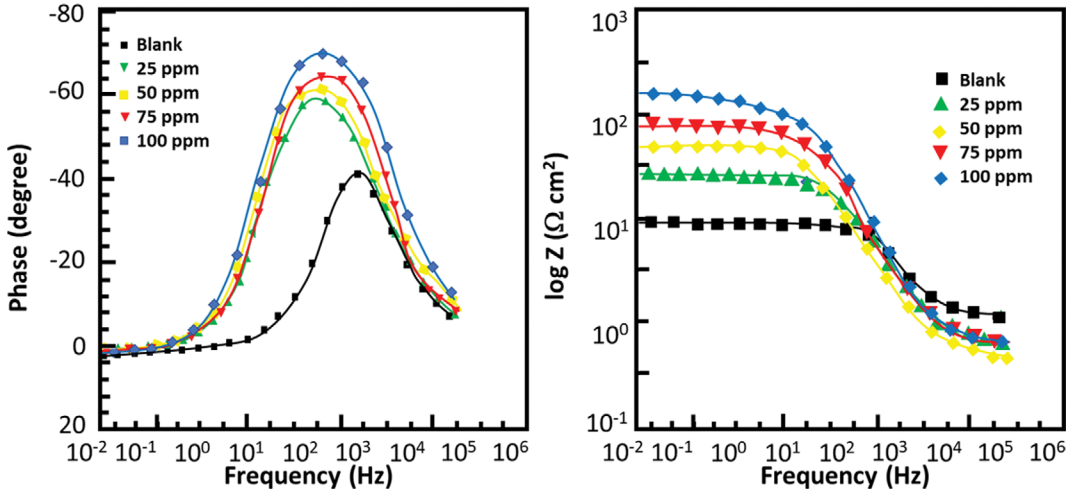

Fig. 6. Bode plots for corrosion of mild steel in 0.5 M HCl without and with various concentrations of MBSB molecules.

Table 4. EIS parameters for the corrosion of mild steel in 0.5 M HCl with and without MBSB inhibitor molecules at various concentrations

Inhibitor	C (mM)	R_s (Ω cm^2)	R_p (Ω cm^2)	n	IE%	θ
Blank		1.13	10.71	0.826		
MBSB	25	0.585	33.01	0.841	67.56	0.67
	50	0.539	61.84	0.847	82.69	0.82
	75	0.548	90.14	0.847	88.12	0.87
	100	0.563	172.98	0.853	93.80	0.93

Table 5. DFT parameters for neutral and protonated form of MBSB inhibitor molecule

MBSB	E_{HOMO} (eV)	E_{LUMO} (eV)	ΔE (eV)	η (eV)	σ (eV)	χ (eV)	ΔN (eV)	μ (Debye)
Neutral	−0.24	−0.08	0.16	0.08	12.5	0.16	0.409	4.94

which is typically indicated by Z_{CPE}.

$$Z_{CPE} = Y_0^{-1}((i\omega)^n)^{-1} \quad (9)$$

where the letters, ω, Y_0, n, and i, respectively, stand for the angular frequency, the CPE constant, the phase shift, and an imaginary number. Since a high value of n correlates with a high level of surface smoothness and vice versa, it can also be used as a measure of surface roughness or smoothness [41]. Table 4 lists the calculated impedance parameters, % inhibition efficiencies, and surface coverages. The results show that, with the exception of a few, n values are higher in the inhibited solution than in the uninhibited condition. This discovery shows that the metallic surface is substantially smoother in the presence of MBSB, especially at their greater concentration, than it is in the absence. Additionally, the fact that both the inhibited and uninhibited conditions' n values are close to unity shows that the CPE functions as a pseudo-capacitor during investigation. Organic inhibitors are thought to be able to suppress corrosion in aggressive acidic media by adsorption on metal-electrolyte interfaces, which leads to the formation of an electric double layer [1,42]. The findings in Table 4 demonstrate that R_{ct} values for the inhibited case are much greater than those for the non-inhibited condition. This result suggests that the difficulty of charge transfer in the presence of MBSB is due to their adhesion to the metal-electrolyte interfaces. According to additional findings, increase in R_{ct} value is much more noticeable at greater inhibitor concentrations.

6. Computational Studies

Fig. 7 depicts the frontier molecular orbitals (optimized, HOMO, LUMO and MEP) of the MBSB, while Table 5 lists numerous calculated DFT indices. The DFT parameters in the table are in good agreement with the outcomes of the experimental data. Generally, interactions of corrosion inhibitors on the metallic surface comprise donor-acceptor bonding; during these interactions, E_{HOMO} is associated with the inhibitor's capacity to transmit electrons (charge), while E_{LUMO} is associated with the inhibitor's ability to accept electrons. Hence, strong metal-inhibitor bindings and good protective ability are related with high values of E_{HOMO} and low values of E_{LUMO} [43-47]. The highest occupied-molecular-orbital (E_{HOMO}) energy shows the capability of the tested inhibitor to donate electrons. The capability of the molecules to accept electrons from the back donation of iron, and to thus enhance the binding energy between the metal and the inhibitor, is shown by a lower E_{LUMO} value. The greater the E_{HOMO} and the lower the E_{LUMO}, the better the tested inhibitor's capacity to attach to the metal surface [18,48-51]. This suggests that MBSB is an efficient corrosion inhibitor and is in

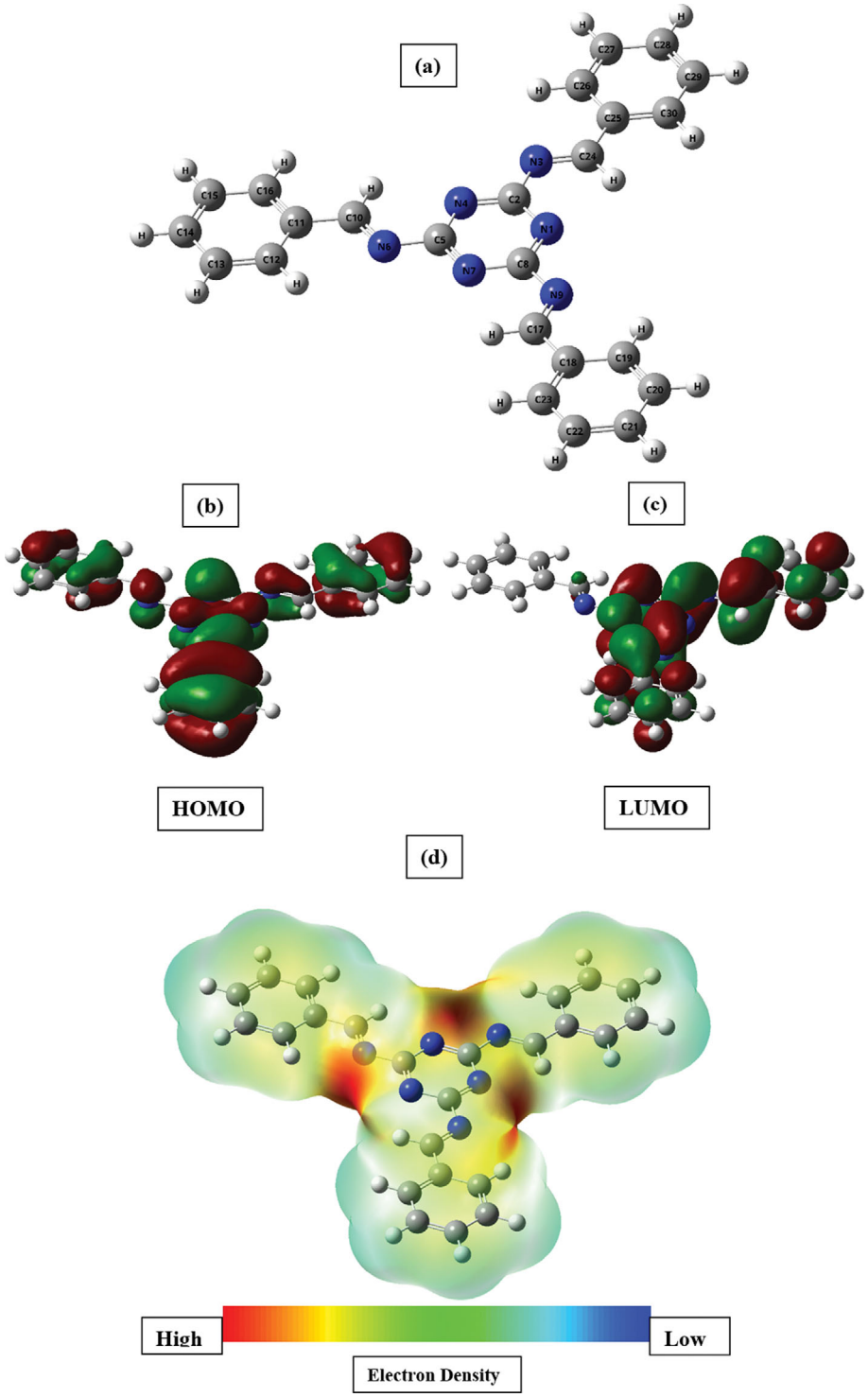

Fig. 7. The optimized chemical structure (a), highest occupied molecular orbital (b), and lowest unoccupied molecular orbital (c), Molecular electrostatic potential (d) of the tested inhibitor MBSB.

good agreement with the experimental findings [52]. The chemical response is determined by the energy gap (Egap) values. In terms of reactivity, the molecule is more reactive towards the substrate surface the higher its inhibitory efficiency, and the smaller the ΔE gap, the more stable it is. As a result, the combination of MBSB with the Fe substrate is stable. The dipole moment (μ) is caused by the nonuniform surface charge distribution of the molecule's atoms [53]. The low value of the dipole moment supports the inhibitor molecule. The soft molecule in the hard-soft acid-base concept has lower Egap values and greater basicity, whereas the converse is true when comparing the hard molecules [54]. As a result, the soft molecule has more adsorption ability due to its easier electron

transfer, and it is a stronger corrosion inhibitor than the hard molecule.

According to Lukovit's research, when the number of electrons transmitted (ΔN) is less than 3.6, the inhibition performance improves as a function of the electron transfer [54-56]. The larger the fraction of electron transport (ΔN), the better is the corrosion inhibitor. The high value of ΔN for MBSB suggests that it is a good corrosion inhibitor and electron donor.

The global electronegativity value for the MBSB was also computed. A high value of global electronegativity (χ) suggests that undertaken compound is less potent to donate/transfer its electron to the appropriate acceptor molecule, e.g., d-orbital of the surface Fe atoms in the present case.

The MBSB shows the electronegativity value of 0.16. The low value of χ for MBSB indicates that it has high ability of the electron transfer, thereby acts as good corrosion inhibitor. Based on the values of E_{LUMO} and E_{HOMO}, global hardness (η) and softness (σ) values were also derived for MBSB molecule. The high value of σ is related to high reactivity; electron donating ability, adsorption tendency and inhibition efficiency, and the converse is true for η [54,57]. Results showed that MBSB has a high value of σ (12.5 eV) and low value of η (0.08 eV), which suggested that MBSB highly reactive and potent corrosion inhibitor. On the basis of the above discussion, it can be concluded that DFT study provides good support to the experimental results and findings.

7. Suggested Corrosion-Inhibition Mechanism

The inhibitory inertia of organic molecules is caused by the formation of a protective layer that is adsorbed onto the iron surface. Gravimetric measurements revealed that the tested inhibitor greatly reduced mild-steel corrosion. Moreover, the adsorption isotherm studies reveal that the investigated inhibitor molecules adhere to the mild-steel surface and follow the Langmuir adsorption model. Furthermore, the generated protective film's adsorption behavior is principally determined by (1) electrostatic interactions through protonated heteroatoms, and (2) different linkages between inhibitor molecules and the mild-steel surface [58].

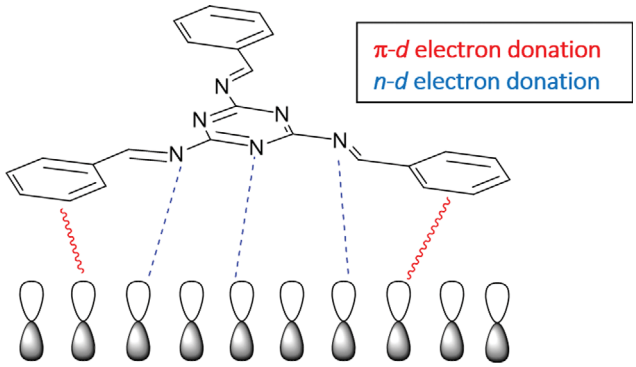

Fig. 8. Suggested corrosion-inhibition mechanism of mild steel in 0.5 M HCl with the addition of the examined inhibitor (MBSB).

Fig. 8 illustrates in further detail how the tested inhibitor compounds interacted with the mild-steel surface. The most common procedure of adsorption between the inhibitor molecule and the mild-steel surface involves the interaction of both the pi-electrons of the aromatic rings and the vacant d-orbital of the metal atoms. The second method involves interactions between the lone electron pairs in the heteroatoms and the unoccupied d-orbitals on the surface of iron (mild steel) atoms. The d-orbitals of the Fe atom

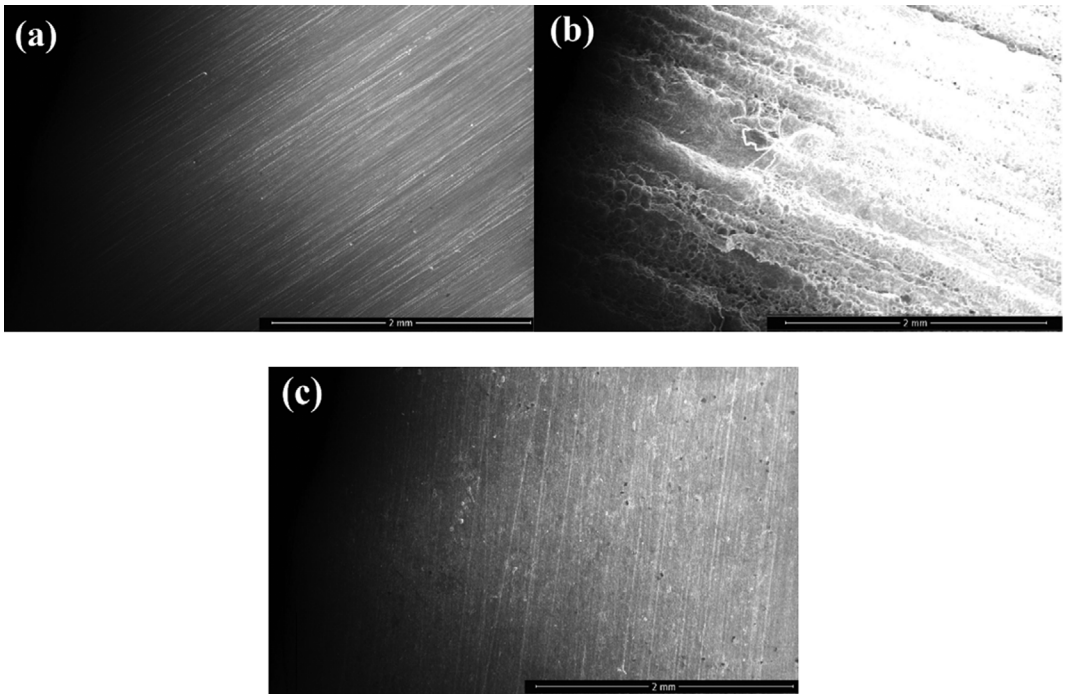

Fig. 9. SEM image of corroded mild steel specimen for 4 h immersion time in the (a) before Immersion (polished), (b) in 0.5 M HCl without inhibitor (c) with 75 ppm MBSB.

will share these active electrons.

8. Morphological Investigation

To confirm the adsorption of the inhibitor on the mild steel surface in the presence and absence of inhibitor, scanning electron microscopy (SEM) experiments were carried out. Fig. 9 displays the SEM images of mild steel specimen that corroded for three hours. As can be seen from extremely rough surface and visible pits and fissures, the unprotected metallic specimens in SEM photos are severely corroded and damaged. However, as can be seen from their SEM image, the metallic surface is greatly improved in the presence of synthesized MBSB inhibitor. It can be postulated that MBSB generate surface films that shield metallic surfaces from corrosion based on the better surface morphologies of the shielded metallic specimens. This result also confirmed the pattern of inhibitory effectiveness attained through weight loss and electrochemical techniques.

CONCLUSION

Novel melamine-benzaldehyde hybrid tris-Schiff base (MBSB) corrosion inhibitor was synthesized and its potential investigated to function as mixed-type inhibitor. The synthetic inhibitor demonstrated high mild steel inhibition performance in 0.5 M HCl. According to the evaluation of weight loss, the efficacy of inhibition increased as inhibitor concentration increased and reduced as temperature increased; and maximum efficiency of 94.78% was derived for MBSB. According to electrochemical impedance measurements, the increased inhibition efficacy 99.34% of the inhibitor solutions was caused by their high charge transfer resistance values. The Langmuir type of isotherm was identified through the analysis of adsorption isotherms and thermodynamic parameters, indicating physisorption. A polarization analysis revealed that MBSB functions primarily as a cathodic type inhibitor. Further evidence for the synthetic tris-Schiff base's ability to suppress corrosion was provided by the SEM pictures, which showed the development of a protective layer on the surface of mild steel.

ACKNOWLEDGEMENTS

The work was funded by the Researchers Supporting Project Number (RSPD2023R763) King Saud University, Riyadh, Saudi Arabia.

CONFLICTS OF INTEREST

There are no conflicts to declare.

REFERENCES

1. I. Arshad, A. Saeed, P. A. Channar, S. A. Shehzadi, M. N. Ahmed and M. Siddiq, *RSC Adv.*, **10**(8), 4499 (2020).
2. L. Guo, S. Kaya, I. B. Obot, X. Zheng and Y. Qiang, *J. Colloid Interface Sci.*, **506**, 478 (2017).
3. N. Chafai, S. Chafaa, K. Benbouguerra, D. Daoud, A. Hellal and M. Mehri, *J. Taiwan Inst. Chem. Eng.*, **70**, 331 (2017).
4. N. Chafai, S. Chafaa, K. Benbouguerra, A. Hellal and M. Mehri, *J. Mol. Struct.*, **1181**, 83 (2019).
5. S. Al-Baghdadi, T. Gaaz, A. Al-Adili, A. Al-Amiery and M. Takriff, *Int. J. Low Carbon Technol.*, **16**(1), 181 (2021).
6. A. A. Al-Amiery, *Surf. Rev. Lett.*, **28**(03), 2050058 (2021).
7. K. Benbouguerra, S. Chafaa, N. Chafai, M. Mehri, O. Moumeni and A. Hellal, *J. Mol. Struct.*, **1157**, 165 (2018).
8. M. Djenane, S. Chafaa, N. Chafai, R. Kerkour and A. Hellal, *J. Mol. Struct.*, **1175**, 398 (2019).
9. B. Tan, B. Xiang, S. Zhang, Y. Qiang, L. Xu, S. Chen and J. He, *J. Colloid Interface Sci.*, **582**, 918 (2021).
10. S. B. Al-Baghdadi, A. A. Al-Amiery, T. S. Gaaz and A. A. H. Kadhum, *Koroze Ochr. Mater.*, **65**(1), 12 (2021).
11. A. Kokalj, *Corros. Sci.*, **196**, 109939 (2022).
12. H. Jafari, M. Rezaeivala, N. Mokhtarian, A. Berisha and E. Ameri, *J. Bio- Tribo-Corros.*, **8**(3), 1 (2022).
13. H. Li, Y. Zhang, C. Li, Z. Zhou, X. Nie, Y. Chen, H. Cao, B. Liu, N. Zhang, Z. Said, S. Debnath, M. Jamil, H. M. Ali and S. Sharma, *Korean J. Chem. Eng.*, **39**(5) 1107 (2022).
14. F. K. Ojo, I. A. Adejoro, J. A. Lori, O. E. Oyeneyin and K. G. Akpomie, *Chem. Afr.*, **5**(4), 943 (2022).
15. A. Bimoussa, Y. Koumya, A. Oubella, Y. Kaddouri, M. Fawzi, Y. Laamari, A. Abouelfida, M. Y. A. Itto, R. Touzani and A. Benyaich, *J. Mol. Struct.*, **1253**, 132276 (2022).
16. M. M. El-Hendawy, A. M. Kamel and M. M. Mohamed, *Phys. Chem. Chem. Phys.*, **24**(2), 743 (2022).
17. Y. Hou, L. Zhu, K. He, Z. Yang, S. Ma and J. Lei, *J. Mol. Liq.*, **348**, 118432 (2022).
18. A. S. Jasim, K. H. Rashid, K. F. Al-Azawi and A. A. Khadom, *Results Eng.*, **15**, 100573 (2022).
19. A. Imjjad, K. Abbiche, M. D. Mellaoui, A. Jmiai, N. El Baraka, A. A. Taleb, I. Bazzi, S. El Issami, M. Hilali and R. B. Said, *Appl. Surf. Sci.,* **576**, 151780 (2022).
20. C. Verma, J. Haque, E. E. Ebenso and M. A. Quraishi, *Results Phys.*, **9**, 100 (2018).
21. Y. Zeng, L. Kang, Y. Wu, S. Wan, B. Liao, N. Li and X. Guo, *J. Mol. Liq.*, **349**, 118108 (2022).
22. K. R. Ansari, M. A. Quraishi and A. Singh, *Corros. Sci.*, **95**, 62 (2015).
23. H. A. El-Ghamry, A. Fawzy, T. A. Farghaly, T. M. Bawazeer, N. Alqarni, F. M. Alkhatib and M. Gaber, *Arab. J. Chem.*, **15**(1), 103522 (2022).
24. A. A. Al-Amiery, W. K. Al-Azzawi and W. N. R. W. Isahak, *Sci. Rep.*, **12**(1), 17773 (2022).
25. N. Z. N. Hashim, K. Kassim, H. M. Zaki, A. I. Alharthi and Z. Embong, *Appl. Surf. Sci.*, **476**, 861 (2019).
26. D. S. Chauhan, M. J. Mazumder, M. Quraishi and K. Ansari, *Int. J. Biol. Macromol.*, **158**, 127 (2020).
27. P. Shetty, *Chem. Eng. Commun.*, **207**(7), 985 (2020).
28. B. S. Mahdi, M. K. Abbass, M. K. Mohsin, W. K. Al-Azzawi, M. M. Hanoon, M. H. H. Al-Kaabi, L. M. Shaker, A. A. Al-Amiery, W. N. R. W. Isahak and A. A. H. Kadhum, *Molecules*, **27**(15), 4857 (2022).
29. C. M. Fernandes, V. G. Pina, C. G. Alfaro, M. T. de Sampaio, F. F. Massante, L. X. Alvarez, A. M. Barrios, J. C. M. Silva, O. C. Alves and M. Briganti, *Colloids Surf. A: Physicochem. Eng.*, **641**, 128540 (2022).
30. V. K. Thomas, J. K. Thomas, V. P. Raphael, K. Ragi, R. Johnson and R. Babu, *J. Bio- Tribo-Corros.*, **7**(3), 1 (2021).

31. M. Frisch, http://www.gaussian.com/ (2009).
32. C. Lee, W. Yang and R. G. Parr, *Phys. Rev. B.*, **37**(2), 785 (1988).
33. M. A. Bedair, A. M. Abuelela, W. M. Zoghaib and T. A. Mohamed, *J. Mol. Struct.*, **1244**, 130927 (2021).
34. H. H. Tran, T. H. Nguyen, T. T. Tran, H. D. Vu and H. M. T. Nguyen, *ACS Omega*, **6**(32), 20975 (2021).
35. I. Arshad, S. Ashraf, A. Abbas, S. Hameed, K. M. Lo and M. M. Naseer, *Eur. Chem. Bull.*, **3**, 587 (2014).
36. M. Mirzaei-Saatlo, H. Jamali, S. Moradi-Alavian, E. Asghari, R. Teimuri-Mofrad and M. D. Esrafili, *Mater. Chem. Phys.,* **293**, 126895 (2023).
37. R. Sanmugapriya, S. Peters, E. Varathan, R. Monisha and J. A. Selvi, *Colloids Surf. A: Physicochem. Eng. Asp.*, **661**, 130919 (2023).
38. A. Bouoidina, R. Haldhar, R. Salim, E. Ech-chihbi, H. Ichou, F. El-Hajjaji, S.-C. Kim, B. El Ibrahimi, S. Kaya and M. Taleb, *Korean J. Chem. Eng.,* **40**(1), 235 (2023).
39. S. Melhi, M. A. Bedair, E. H. Alosaimi, A. A. Younes, W. H. El-Shwiniy and A. M. Abuelela, *RSC Adv.*, **12**(50), 32488 (2022).
40. L. Ma, W. Lu, D. Yang, J. Shen, Z. Gao, S. Zhang and Q. Liao, *Sustain. Chem. Pharm.*, **22**, 100488 (2021).
41. S. Satpati, A. Suhasaria, S. Ghosal, S. Dey and D. Sukul, *Mater. Chem. Phys.*, **296**, 127200 (2023).
42. A. G. Kalkhambkar and S. Rajappa, *Chem. Eng. J. Adv.*, **12**, 100407 (2022).
43. A. Saeed, M. Ifzan Arshad, M. Bolte, A. C. Fantoni, Z. Y. Delgado Espinoza and M. F. Erben, *Spectrochim. Acta - A: Mol. Biomol. Spectrosc.*, **157**, 138 (2016).
44. A. Saeed, I. Arshad and U. Flörke, *J. Chem.*, **2013**, 648121 (2013).
45. M. N. Ahmed, I. Arshad, W. Bo, S. Hameed, B. A. Khan, K. A. Yasin and M. M. Naseer, *Chin. J. Struct. Chem.*, **33**(12), 1749 (2014).
46. I. Arshad, J. Yameen, A. Saeed, J. M. White and F. Albericio, *Crystals*, **7**(1), 19 (2017).
47. A. Saeed, I. Arshad and U. Flörke, *J. Struct. Chem.*, **56**(2), 396 (2015).
48. S. K. Ahmed, W. B. Ali and A. A. Khadom, *Int. J. Ind. Chem.*, **10**(2), 159 (2019).
49. A. Shareef Jasim, A. A. Khadom, K. H. Rashid and K. F. Al-Azawi, *Results Chem.*, **4**, 100569 (2022).
50. A. A. Fadhil, A. A. Khadom, H. Liu, C. Fu, J. Wang, N. A. Fadhil and H. B. Mahood, *J. Mol. Liq.*, **276**, 503 (2019).
51. L. Ouksel, R. Bourzami, S. Chafaa and N. Chafai, *J. Mol. Struct.*, **1222**, 128813 (2020).
52. H. R. Obayes, A. A. Al-Amiery, G. H. Alwan, T. A. Abdullah, A. A. H. Kadhum and A. B. Mohamad, *J. Mol. Struct.*, **1138**, 27 (2017).
53. R. Bourzami, L. Ouksel and N. Chafai, *J. Mol. Struct.*, **1195**, 839 (2019).
54. I. Arshad, K. Qureshi, A. S. Saleemi, A. Abdullah, A. A. A. Bahajjaj, S. Ali and A. Bokhari, *RSC Adv.*, **13**(28), 19301 (2023).
55. O. Moumeni, S. Chafaa, R. Kerkour, K. Benbouguerra and N. Chafai, *J. Mol. Struct.*, **1206**, 127693 (2020).
56. S. Mammeri, N. Chafai, H. Harkat, R. Kerkour and S. Chafaa, *Iran. J. Sci. Technol. Trans. A: Sci.*, **45**(5), 1607 (2021).
57. A. Zarrouk, B. Hammouti, A. Dafali, M. Bouachrine, H. Zarrok, S. Boukhris and S. S. Al-Deyab, *J. Saudi Chem. Soc.*, **18**(5), 450 (2014).
58. N. Assad, F. Abdul-Hameed, E. Yousif and A. Balakit, *Al-Nahrain J. Sci.*, **18**(2), 69 (2015).